Research Article

Simulation of Multiphase Flow and Mixing in a Conveying Element of a Co-Rotating Twin-Screw Extruder by Using SPH

Tianwen Dong [ID],[1] Jianchun Wu,[1] Yufei Ruan,[1] Jiawen Huang,[1] and Shiyu Jiang[2]

[1]*Jiangxi Province Key Laboratory of Polymer Preparation and Processing, Shangrao Normal University, Shangrao 334001, China*
[2]*Jiangxi Province Key Laboratory of Precision Drive & Control, Nanchang Institute of Technology, Nanchang 330099, China*

Correspondence should be addressed to Tianwen Dong; tianwendong@live.cn

Multiphase flows and mixing in partially filled conveying elements of twin-screw extruders (TSEs) were simulated by using smoothed-particle hydrodynamics (SPH). A validation of SPH using experiment from the literature for a co-rotating twin-cam mixer indicated good agreement. A two-phase Poiseuille flow was also used to validate the accuracy of our approach. The results of two-phase flow in TSE show that the viscosity ratio significantly affects the flow and mixing of two-phase fluids. The symmetry of flow field is broken with different parameters. In the full filled case, the pressure squeezes particles into the gap, which is conducive to improve the performance of mixing of fluids. On the contrary, in the partially filled case, because there is no background pressure, particles tend to bypass the gap and flow to the cavity of the chamber. This work laid a foundation for further study of polymer blending by simulation.

1. Introduction

Multiphase flow phenomena can be frequently found in variety of nature and industrial processes, such as sedimentation processes in rivers [1], casting [2], and screw extrusion [3].

As excellent mixing equipment, co-rotating, intermeshing twin screw extruder is widely used in polymers, food, and pharmaceutical industries. Multimaterial flows and mixing with sharp immiscible interfaces often occur in TSE in processing operations. In addition, some complex situations also need to be considered, such as complex geometry, non-Newtonian fluids, and partially filled regions.

The early simulation technology for twin screw extrusion mainly refers to the one-dimensional (1D) analysis method based on lubrication theory [4]. In this method, the extruder is unwound along the channel, and only the mean value of parameters along the axial can be obtained. In recent decades, numerical analysis technology has achieved unprecedented improvement with the rapid progress of computer technology. Among them, the representative

computational fluid dynamics (CFD) methods, such as finite difference (FD) [5], finite element method (FEM) [6, 7], and finite volume method (FVM) [8], have been widely used in the simulation of screw extrusion. Because FD needs structured grids and FEM and FVM adopt structured grids, unstructured grids, or hybrid grids, the latter two are mostly used in the current commercial software, such as Polyflow and Fluent (both are integrated in Ansys). At present, the method for handling complex geometry with rotating boundaries is very mature, for example, the MST (mesh superposition technique) [6, 7]. For mesh-based methods, to track the interface between phases, some special techniques, such as the volume-of-fluid (VOF) and level-set method, are required [9, 10]. The VOF method is robust, but the captured interface usually spans several grid cells. In level-set method, the interface can be sharply captured, but there is a problem in mass conservation [11]. Because of the limitation of the mesh-based methods, the current researches mainly focus on the mixing of a single fluid, which means the fluid mixes with itself [7]. Based on the above reason, the current characterization of dispersive mixing mainly adopts the microscopic imaging technology or calculation of mixing

index, which includes some information of extensional stress and shear stress [12].

In recent years, a meshless method, smoothed-particle hydrodynamics (SPH), is attracting an increasing attention of scientists and engineers [13–15]. For its excellent adaptive property, it is very suitable for simulating complex flow, such as a free surface flow or multiphase flow [16–18]. So far, SPH has been used to study the flow and mixing in screw extrusion. The early research studies mainly focused on how to improve SPH in the following aspects: calculation accuracy, stability, boundary treatment, and computational efficiency [19–23]. Recently, some researchers tried to promote more in-depth application of SPH in the field of extrusion. For example, Khinast and his co-workers investigated the pressure build-up, power consumption, dissipation, and distributive mixing behavior using SPH [24, 25]. The most current research studies attempted to use SPH to simulate a free surface flow in TSE and mainly aimed at single-phase flow [19–26].

In this work, we studied multiphase flow and mixing in TSE by using SPH. Full filled and partially filled models were both studied. The governing equations and SPH method are introduced in Sections 2 and 3, respectively. In Section 4, the SPH simulation is validated against the mixing experiment performed by Avalosse and Crochet [27]. In Section 5, a two-phase Poiseuille flow is also used to test the algorithm. In Section 6, we analyze the two-phase flow and mixing in a TSE. The conclusions are presented in Section 7.

2. Governing Equations

The Navier–Stokes equations written in Lagrangian form are given by

$$
\frac{D\rho}{Dt} = -\rho \nabla \cdot \mathbf{v},
$$
$$
\frac{D\mathbf{v}}{Dt} = -\frac{1}{\rho} \nabla p + \frac{1}{\rho} \nabla \cdot \boldsymbol{\tau} + \mathbf{F}. \tag{1}
$$

Here ρ, $\mathbf{v}$, p, and $\mathbf{F}$ are the density, velocity vector, pressure, and a body force, respectively. τ is the shear tensor; $\tau = 2\mu\varepsilon - 2/3\mu(\nabla \cdot \mathbf{v})\mathbf{I}$, $\varepsilon = 1/2[\nabla\mathbf{v} + (\nabla\mathbf{v})^T]$.

3. SPH Method

The basic principle of the SPH formulation is the kernel approximation of a function f which represents a field variable defined over a support domain of a particle [14]. It can be written as

$$
f(r_\mathbf{i}) = \sum_{j=1}^{N} \mathbf{f}(r_\mathbf{j}) \mathbf{W}(r_\mathbf{i} - r_\mathbf{j}, h) \frac{m_j}{\rho_j}, \tag{2}
$$

where m_j and ρ_j are the mass and density of particle j. r_i and r_j represent position of particles i and j, $\mathbf{r}_{ij} = r_i - r_j$. $W_{ij} = W(r_i - r_j, h)$ is the kernel function, and h is the smooth length to determine the size of the support region.

In this work, the cubic spline kernel with compact support of $1.2\,h$ has been used [28].

$$
W(R, h) = \alpha_d \times
\begin{cases}
\dfrac{2}{3} - R^2 + \dfrac{1}{2}R^3, & 0 \le R < 1; \\[2mm]
\dfrac{1}{6}(2 - R)^3, & 1 \le R < 2; \\[2mm]
0, & R \ge 2,
\end{cases} \tag{3}
$$

where $R = |r_i - r_j|/h$, the normalisation constant $\alpha_d = 15/(7\pi h^2)$ in two-dimension (2D), and $\alpha_d = 3/(2\pi)h^3$ in three-dimension (3D).

For incompressible fluids, the SPH form of the mass and momentum conversation equations for particle i is [29]

$$
\frac{d\rho_i}{dt} = \sum_{j=1}^{N} m_j \mathbf{v}_{ij} \cdot \nabla_i W_{ij}, \tag{4}
$$

$$
\frac{D\mathbf{v}_i}{Dt} = -\sum_{j=1}^{N} m_j \left(\frac{p_i}{\rho_i^2} + \frac{p_j}{\rho_j^2} \right) \nabla_i W_{ij} + \sum_{j=1}^{N} \frac{m_j(\mu_i + \mu_j)\mathbf{r}_{ij} \cdot \nabla_i W_{ij}}{\rho_i \rho_j \left(|\mathbf{r}_{ij}|^2 + 0.01h^2 \right)} \mathbf{v}_{ij} + \mathbf{F}, \tag{5}
$$

where the quantity $\nabla_i W_{ij}$ is the gradient of the kernel, $\mathbf{v}_i$ denotes the velocity of particle i, $\mathbf{v}_{ij} = v_i - v_j$, and μ is dynamic viscosity coefficient.

An artificial density diffusion term is added to the RHS of equation (4) to improve accuracy. It is written as

$$
2\xi hc \sum_{j=1}^{N} (\rho_i - \rho_j) \frac{\mathbf{r}_{ij} \cdot \nabla_\mathbf{i} W_{\mathbf{ij}}}{\mathbf{r}_{ij}^2 + 0.01h^2} \frac{m_j}{\rho_j}, \tag{6}
$$

where coefficient $\xi = 0.1$ is used.

A quasi-compressible approach is used to calculate the pressure directly from the density using an equation of state [30]:

$$
p = B\left[\left(\frac{\rho}{\rho_0} \right)^{\beta} - 1 \right] + p_0, \tag{7}
$$

where ρ_0, ρ_0, c, and p_0 are the density, reference density, sound speed, and background pressure, respectively. $\beta = 7$, $B = c^2\rho_0/\beta$.

Usually, a criterion to estimate sound speed c is needed to satisfy [29]

$$c^2 \geq \frac{1}{\delta}\left(V_0^2, \frac{\nu V_0}{L_0}, \mathbf{F}L_0\right), \quad (8)$$

where V_0, ν, and L_0 are the velocity scale, kinematic viscosity, and length scale, respectively. $\delta = 0.01$ indicates that the density fluctuation is less than 1%.

The governing equations are integrated in time using a two-stage symplectic method [31]. The time step is controlled by three stability constraints: the CFL condition, mass force term, and viscous diffusion term [26].

$$\mathrm{d}t = \min \rightleftharpoons \left(0.25\frac{h}{c}, 0.25\min\left(\frac{h}{\mathbf{F}_i}\right)_i^{1/2}, 0.125\frac{h^2}{\nu}\right). \quad (9)$$

A dynamic boundary condition was used to treat the complex surfaces of wall boundary [32]. The boundary particles satisfy the same equations of continuity and state as the fluid particles, but their positions remain unchanged or externally imposed (moving objects like screws). This boundary method has two significant advantages: it is very suitable for irregular boundaries and it simplifies the code.

4. Experimental Validation

In order to validate the method to simulate the mixing in complex machinery, we simulated the mixing experiment of Avalosse and Crochet for a co-rotating twin-cam mixer [27]. A diagram of the twin-cam geometry is shown in Figure 1. The fluid in the experiment was a Newtonian aqueous solution of glucose, with a viscosity of 50 Pa·s and a density of 1500 kg/m³. The speed of counter-clockwise rotating cams is 0.5 rpm, yielding a Reynolds number of the order of 0.001.

The left column of Figure 2 shows four snapshots of the experiment by Avalosse and Crochet during the counter-clockwise rotation of the co-rotating twin-cam mixer for one revolution. The middle and the right columns of Figure 2, respectively, show the FEM simulation by Avalosse and Crochet and SPH simulation by us. The computational domain in SPH consists of 54891 fluid particles and 55583 boundary particles. All particles are arranged in a regular manner. Reference [22] provides a detailed description of how to convert a mesh into particles. 2175 tracer particles are selected as shown in Figure 2(a). Unlike the FEM method, the tracer particles here are real fluid particles that can be selected in postprocessing software, such as ParaView. Pawlowski found that if the Re < 40, the flow field does not depend on the viscosity value in another similar mixer (single screw extruder) [33]. Robinson also reported that because the time scale of the viscous forces is so small compared with the rotating cams, the viscosity has little or no impact on the solution [34]. In order to speed up the
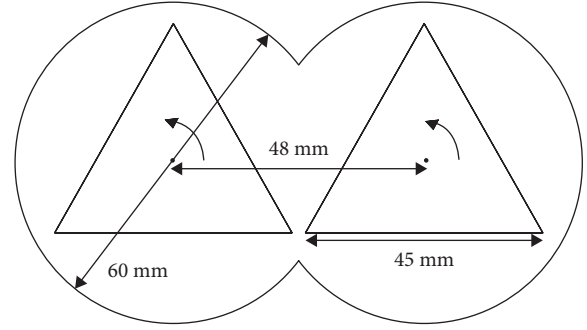

FIGURE 1: Geometry of twin-cam mixer.

calculation, the viscosity in the SPH simulation is set to 10^{-4} of that in the experiment. By comparing the snapshots in Figure 2, the SPH simulation is in good agreement with the experiment and FEM simulation results. As the cams rotate, the tracer particles are divided into two parts by the lower tip of the left cam and the top of the right cam, as shown in Figure 2(b). Subsequently, as they approach the wall, the velocity decreases and they are stretched into the shape of tails. After one revolution, the two parts of particles mix again at the center.

5. Numerical Validation: Two-Phase Poiseuille Flow

As shown in Figure 3, a two-phase Poiseuille flow is performed to study the algorithm's ability to simulate two fluids of different viscosity [35]. The computational domain consists of 3159 fluid particles and 648 boundary particles. Like the single-phase case, two-phase fluids are driven to flow along a 2D channel by a body force $F_x = 10$ m/s². The flow is centered at $y = 0$, and the density and the width of the two phases are equal in this work ($\rho = 1$ kg/m³, $H_1 = H_2 = H = 1$ m). $\mu_1 = 3$ Pa·s; $\mu_2 = 9$ Pa·s. Periodic boundaries are imposed in x direction, and the length is $L = 2H$. Since Reynolds number is very low (less than 0.13), it is unidirectional laminar flow.

The analytical solution for velocity in each phase is [35]

$$u_x = \begin{cases} \dfrac{\rho F_x H^2}{2\mu_1}\left[-\left(\dfrac{y}{H}\right)^2 - \dfrac{\mu_2 - \mu_1}{\mu_1 + \mu_2}\dfrac{y}{H} + \dfrac{2\mu_1}{\mu_1 + \mu_2}\right], & -H \leq y \leq 0, \\[3mm] \dfrac{\rho F_x H^2}{2\mu_2}\left[-\left(\dfrac{y}{H}\right)^2 - \dfrac{\mu_2 - \mu_1}{\mu_1 + \mu_2}\dfrac{y}{H} + \dfrac{2\mu_2}{\mu_1 + \mu_2}\right], & 0 \leq y \leq H. \end{cases}$$

$$(10)$$

Figure 3 also shows the velocity distribution for the fully developed two-phase Poiseuille flow. Unlike the single-phase case, the velocity profile is not symmetric about the center of the channel, which is the interface between the two phases. Figure 4 shows the comparison of SPH results with the analytic solution. The velocity is normalized using the velocity at the center of the channel. The relative error in the average velocity is less than 1%.
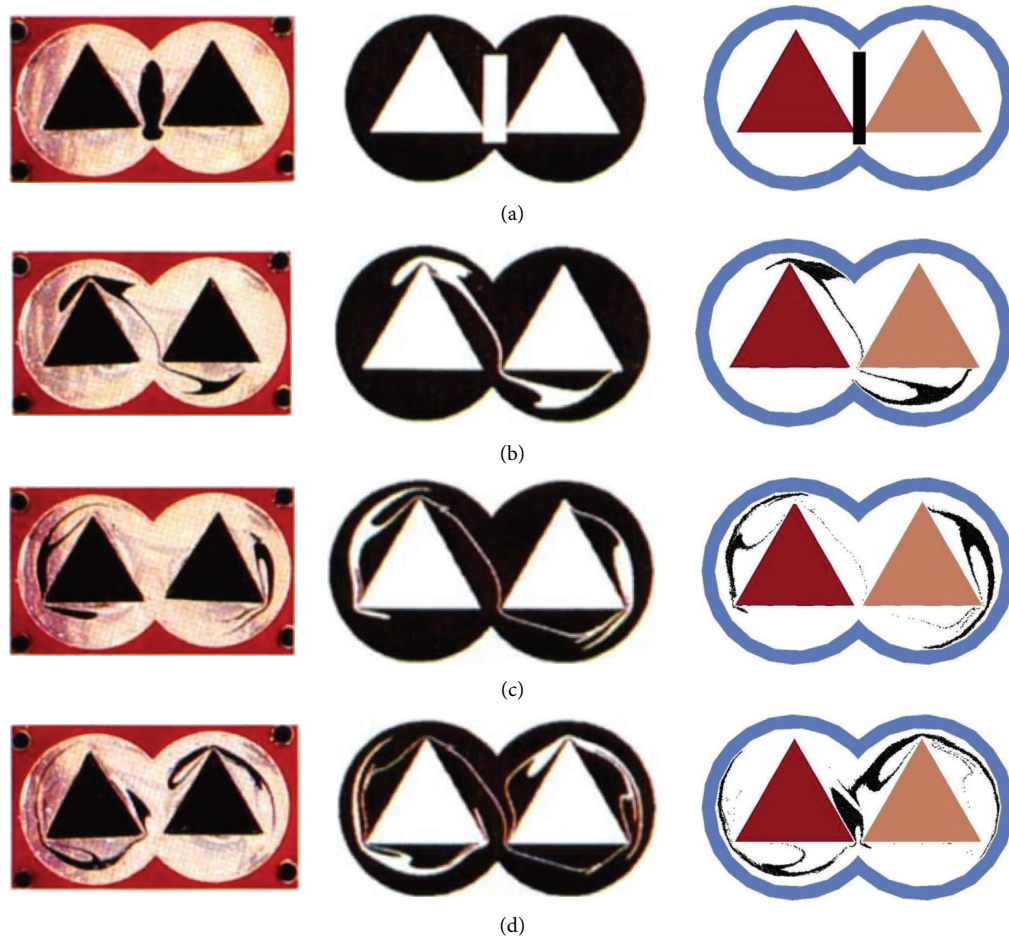
(a)

(b)

(c)

(d)

FIGURE 2: Comparison of experiment by Avalosse and Crochet [27] (left column), FEM simulation by Avalosse and Crochet [27] (middle column), and SPH simulation (right column) during the counter-clockwise rotation of the co-rotating twin-cam mixer for 1 revolution. (a) 0°. (b) 120°. (c) 240°. (d) 360°.
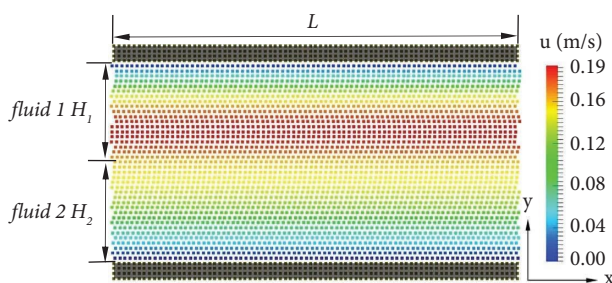

FIGURE 3: Velocity distribution for the fully developed flow.

6. Numerical Results: Two-Phase Flow and Mixing in a TSE

In an industrial co-rotating TSE, numerous screw element types are used, such as conveying element, kneading elements, and specific mixing elements, which are designed to improve the quality of mixing. In order to simplify the problem, we choose the screw conveying element as the research object and assume the flow being Newtonian and isothermal.

Figure 5 shows the geometry of the screw conveying element, which is defined by these parameters:

Number of flights: 2.

Outer screw diameter: 60.0 mm.

Center distance $C = 50.0$ mm.

Screw-barrel clearance $\delta1 = 1.0$ mm (barrel diameter $D = 62$ mm).

Screw-screw clearance $\delta2 = 1.0$ mm.

Table 1 shows the simulation condition for the cases that will be discussed below. Both full filled cases and partially filled cases were studied. In SPH, when starting the simulation, the screws are suddenly rotating at a speed, and the fluid is suddenly pushed from a stationary state. Sometimes (depending on the actual parameters), local cavities may appear, especially in the full filled cases. Therefore, for the full filled cases (case 1 and case 2), a background pressure ($p_0 = 2000$ Pa) is needed to prevent the particles from clustering to form cavities. For the partially filled cases (case 3 and case 4), $p_0 = 0$ Pa. The rotational speed of screws is 60 rpm.
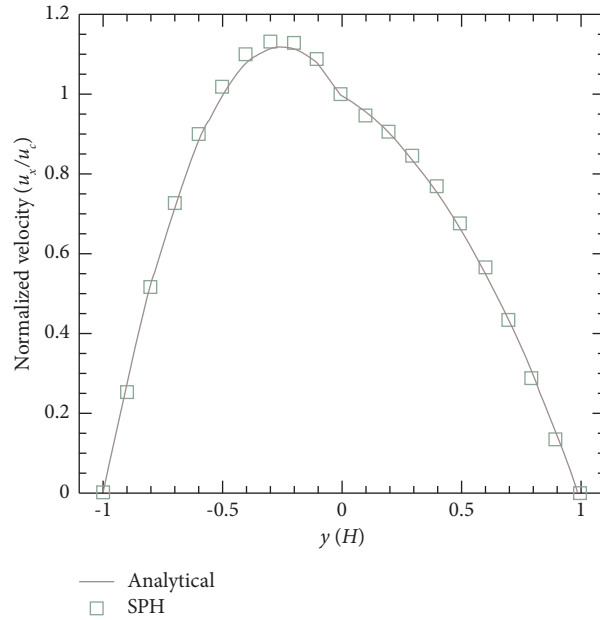
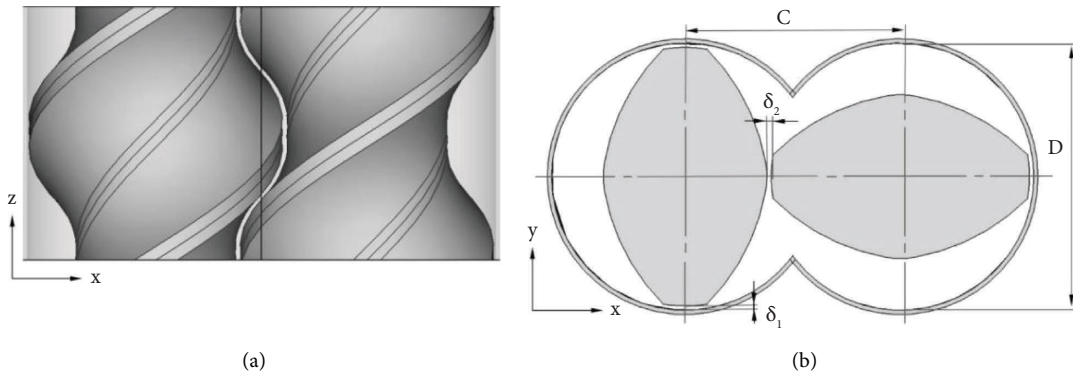FIGURE 4: Velocity profile along channel compared with analytical solution.

FIGURE 5: Geometry of the model. (a) Top view of 3D screw conveying element. (b) Cross section of the screw conveying element.

TABLE 1: Simulation condition.

Case no	State	μ Pa·s Fluid 1	Fluid 2	dx mm	ρ_0 kg/m³	n rpm	p_0 Pa	c m/s	Re —	Number of particles Total	Fluid	Boundary
1	Full filled	1	1				2000			9,990,642	8,824,766	
2		3	1	0.25	1000	60		20	<3.9			1,165,876
3	Half filled	1	1				0			5,563,596	4,397,720	
4		3	1									

The viscosity of fluids in real extrusion, such as polymers and foods, is usually very high (up to 10^4 Pa·s and sometimes even higher), which will lead to extremely small time steps. On the other hand, in order to improve the calculation accuracy, according to Wittek et al.'s suggestion [21], the initial particle spacing (dx) is set to 0.25 mm to ensure that there are at least 4 layers of particles in the clearance. Thus, nearly 10 million particles will be produced with this resolution (see Table 1). It will make the calculation extremely time-consuming (usually in months), even if a parallel SPH algorithm is used [22]. Robinson made a detailed analysis about the effect of viscosity on the calculation [34]. For the very low Reynolds number (much less than 1) in extrusion, the time scale of the viscous forces is very small compared

with the rotating screws, itmeans that the viscous forces have sufficient time to equilibrate the stress field with the moving of the screws. Thus, if the Reynolds number is very low (<40 by our tests), the viscosity can be reduced without affecting the transport of the fluid. In this work, small viscosities of two-phase fluids are used to speed up the integration. As shown in Figure 6, it is assumed that two-phase fluids including fluid 1 (in red) and fluid 2 (in blue) are fed into the chamber at $t = 0$ s. In case 1 and case 3, $\mu_1 = \mu_2 = 1$ Pa·s, in which there is actually only one phase fluid. In case 2 and case 4, $\mu_1 = 3$ Pa·s and $\mu_2 = 1$ Pa·s. For the simulation of multiphase flow, if the density ratio or viscosity ratio is very large (more than 10), numerical instabilities of the standard SPH will become even more serious. Fortunately, the actual viscosity of the two phases is usually very close, which is more conducive to obtain a fine dispersed phase morphology [36]. Therefore, considering the stability of the algorithm, it is reasonable to select the viscosity ratio of 3.

Sometimes, some particles may penetrate the solid boundary because the pressure cannot balance the viscous force. In Eitzlmayer and Khinast's work, an additional repulsive force is applied in the solid boundary [20]. In our recent work, we solved it by setting a higher sound speed [23]. It means that a higher value than that obtained by equation (8) is used. Finally, by some numerical experiments, a sound speed of 20 m/s is set for both cases.

The time step ($dt = 3.75 \times 10^{-6}$ s) is obtained by equation (9). The Reynolds number of the 3D screw conveying element Re $= nD^2\rho/\mu$, where D is the barrel diameter. The body force F is 0 N.

For the periodicity of the geometry, periodic boundary condition is applied in the axis direction. As mentioned in Section 2, the dynamic boundary was used to treat wall boundary. The boundary and the fluid particles are arranged in a regular manner. The initial arrangement of particles was elaborated in detail from 2D and 3D perspectives in reference [22].

Figure 7 shows the comparison of axial velocity in the cross section of the full filled twin screw element during a quarter rotation between case 1 and case 2. The color scale ranges from 0 m/s (blue) to +0.15 m/s (red). An axial velocity of 0 m/s (green) is observed at the walls and also at the rotating screws due to wall adhesion. Moreover, the flow velocities in the intermeshing region are higher than those in the channel. Obviously, two-phase flow breaks the symmetry of velocity distribution. For example, in case 2, the maximum velocities in the right part of the channel are smaller than those in the left part of the channel. On the contrary, in case 1, the maximum velocities in the left part of the channel are very close to those in the right part.

Figure 8 shows the results of mixing after one rotation, which takes case 2 as an example. For a 3D case, in order to see clearly the internal mixing effect, we select 5 cross sections of the element with equal spacing perpendicular to the Z axis. The thickness in the Z-axis direction is set to be 3 mm.
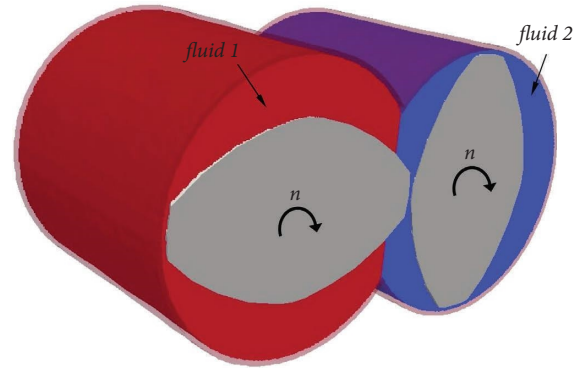

FIGURE 6: Two-phase fluids in the full filled twin screw element at $t = 0$ s.
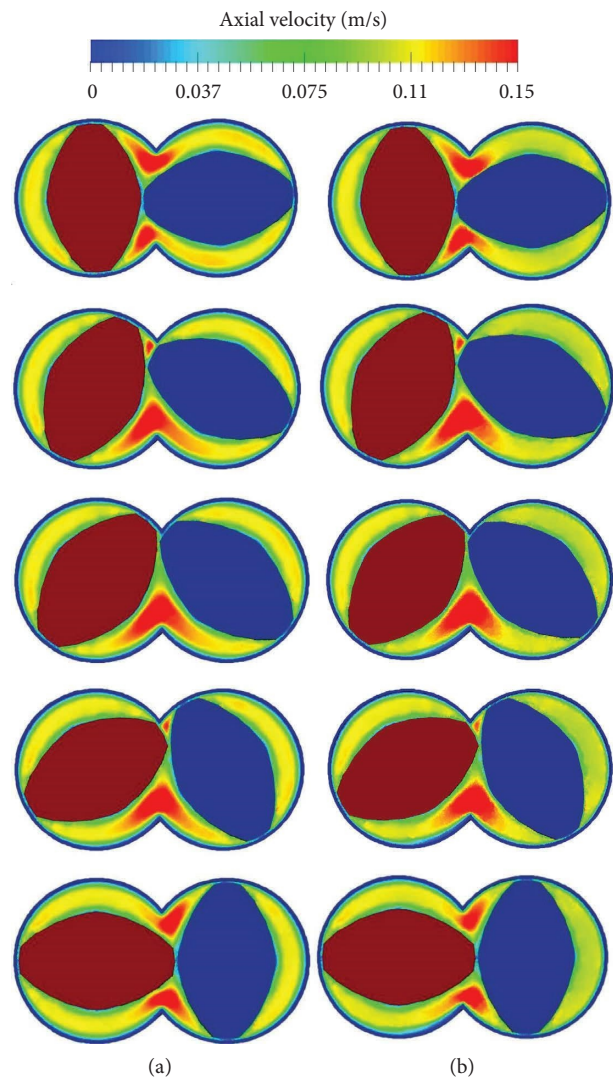

FIGURE 7: Comparison of axial velocity in the cross section of the full filled twin screw element during a quarter rotation between case 1 and case 2 (clockwise rotation) (case 1 results are on the (a); case 2 results are on the (b)).
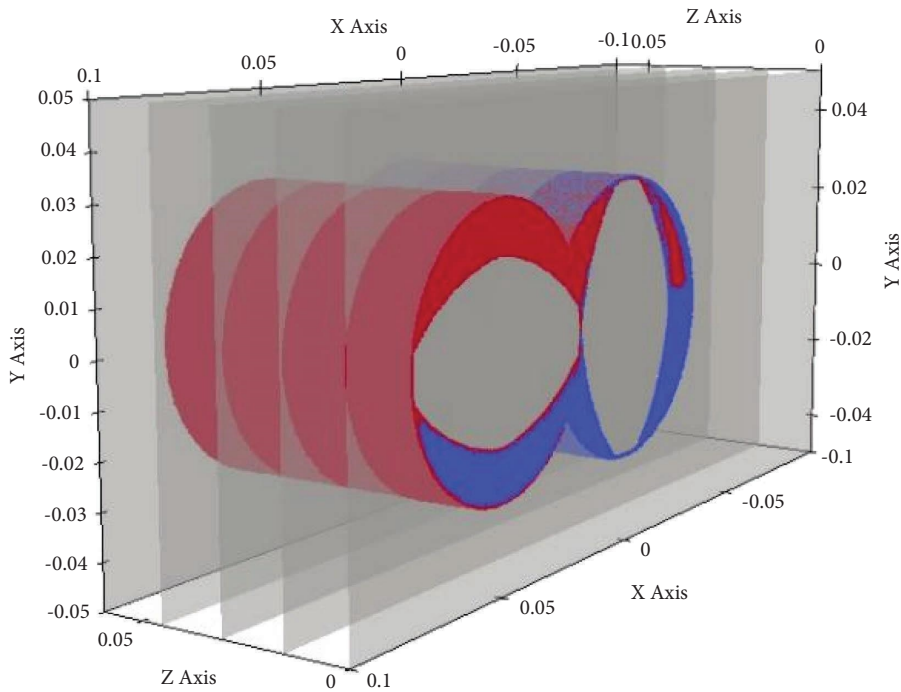
FIGURE 8: The 5 cross sections of the element with equal spacing perpendicular to the Z axis for the results after one rotation.

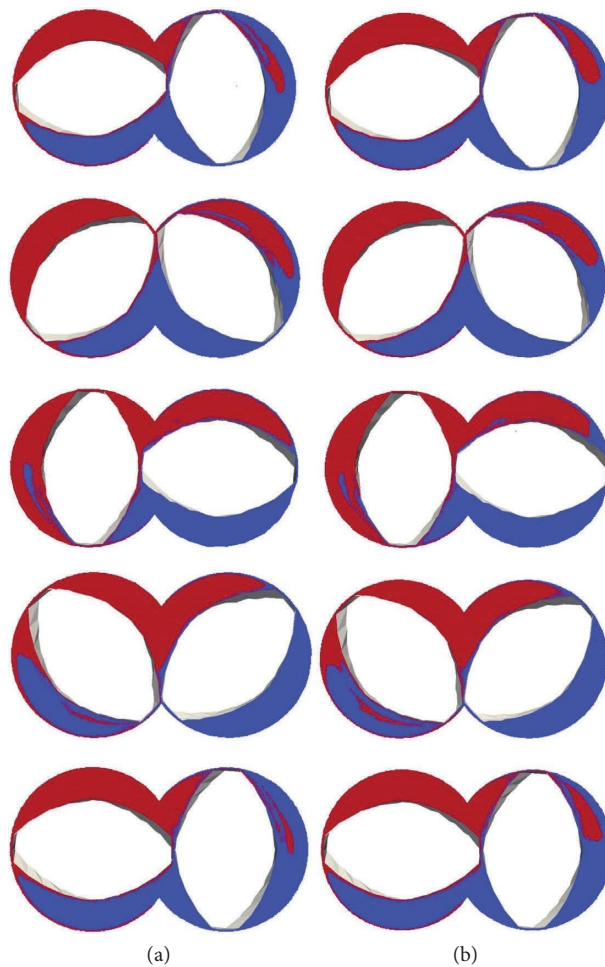(a)   (b)

FIGURE 9: Comparison of the particle distribution after one rotation between the results of case 1 and case 2 corresponding to the 5 sections in Figure 8 ((a) and (b) correspond to case 1 and case 2, respectively).
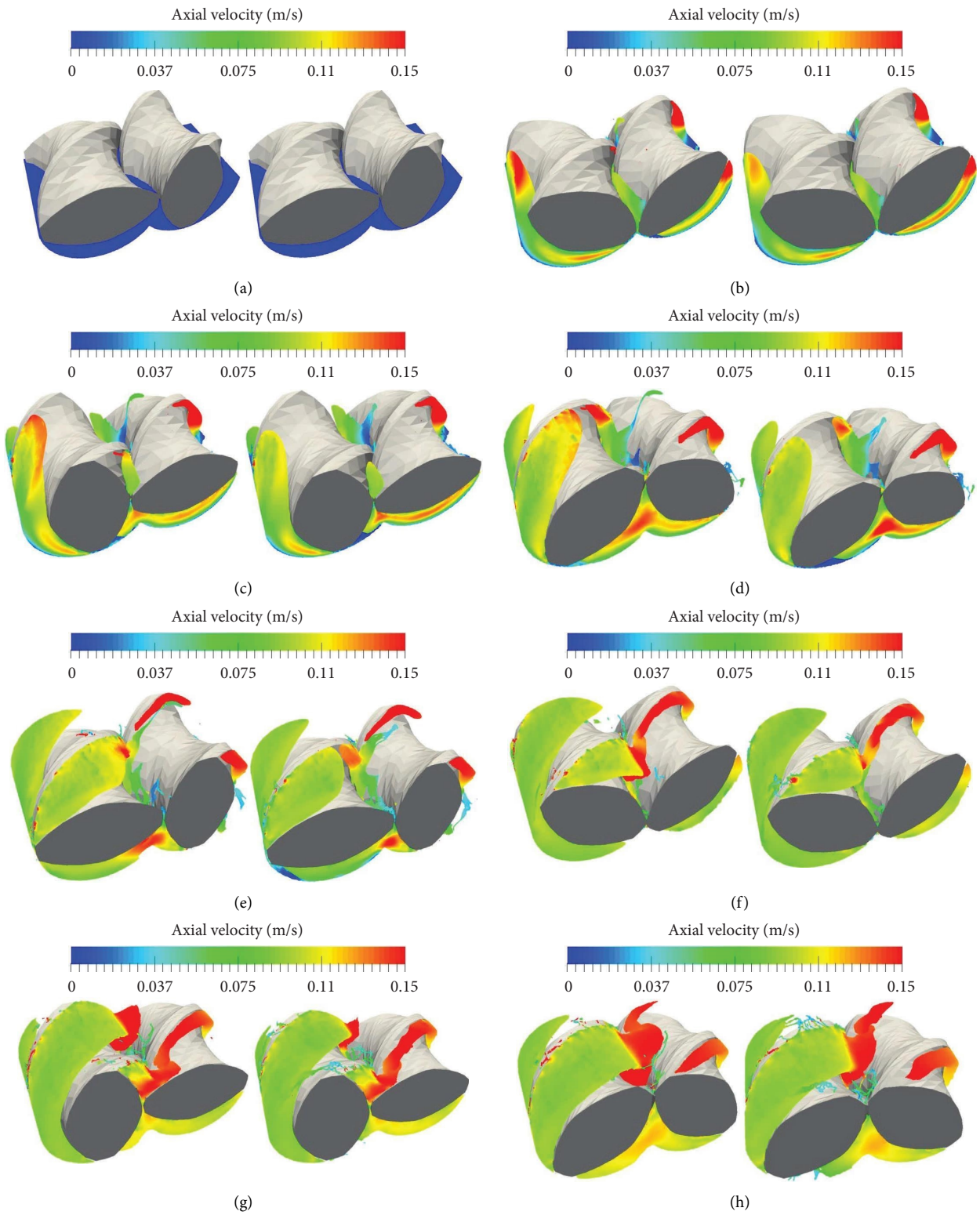
(a)

(b)

(c)

(d)

(e)

(f)

(g)

(h)

Figure 10: Continued.

Axial velocity (m/s)
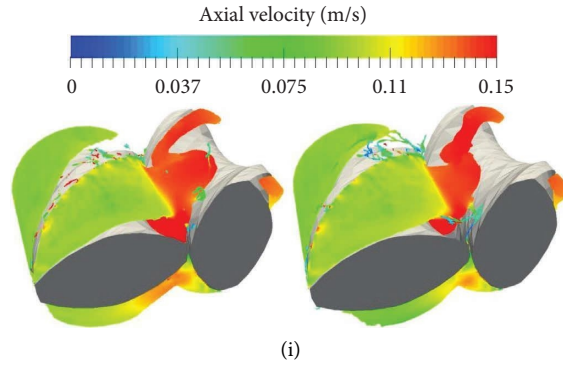
0   0.037   0.075   0.11   0.15

(i)

FIGURE 10: Distributions of particles in a half filled conveying element at different angles in one rotation (clockwise rotation) (results of case 3 are in the left column; results of case 4 are in the right column). (a) 0°. (b) 45°. (c) 90°. (d) 135°. (e) 180°. (f) 225°. (g) 270°. (h) 315°. (i) 360°.

Axial velocity (m/s)

0   0.037   0.075   0.11   0.15

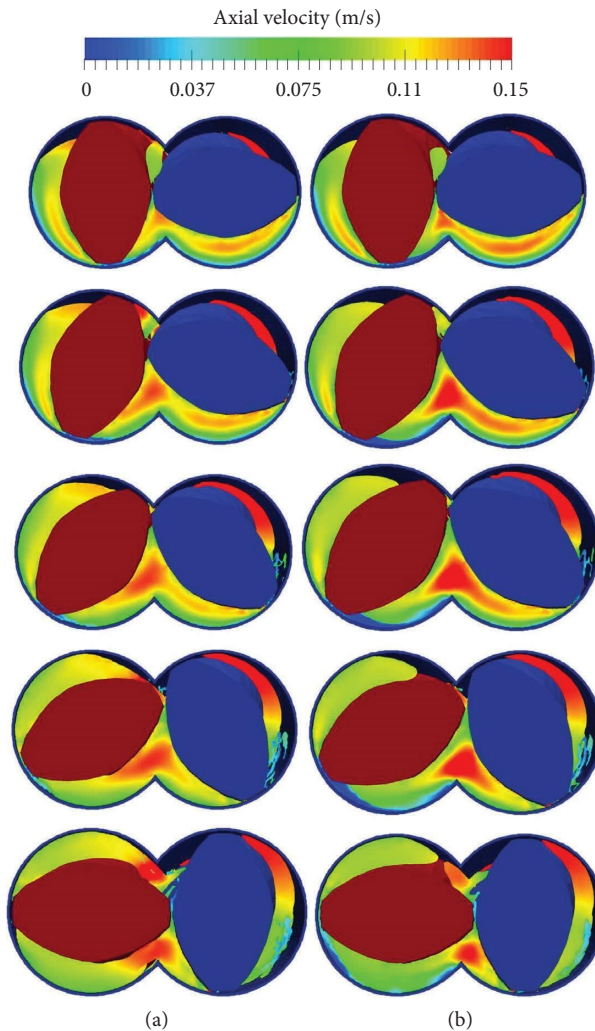(a)   (b)

FIGURE 11: Axial velocity in the cross section of a half filled conveying element during a quarter rotation (clockwise rotation) (results of case 3 are in the (a); results of case 4 are in the (b)).

Figure 9 shows comparison of the particle distribution after one rotation between the results of case 1 and case 2 corresponding to the 5 sections in Figure 8. The left and right columns correspond to the results of case 1 and case 2, respectively. It can be found that after one rotation, the particles are mixed locally for both cases. There is no
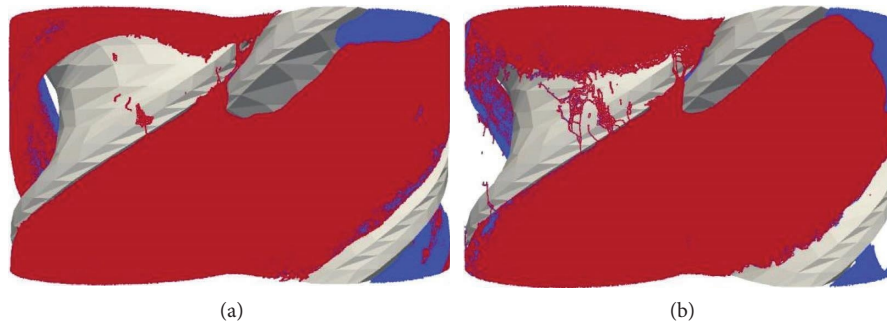
(a)   (b)

FIGURE 12: The top view of particle distribution after 3 rotations between the results of case 3 (a) and case 4 (b).

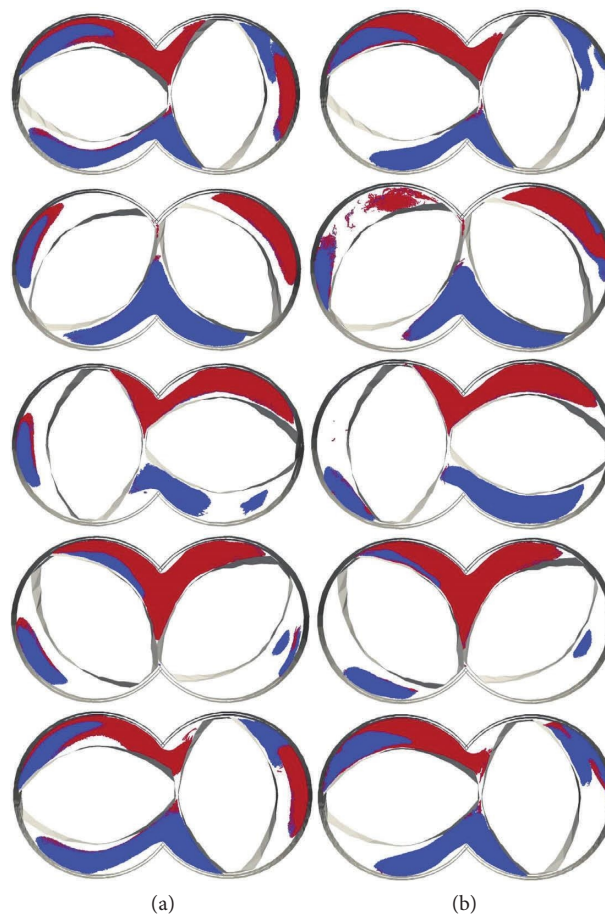(a)   (b)

FIGURE 13: Comparison of the particle distribution after 3 rotations between the results of case 3 and case 4 corresponding to 5 sections shown in Figure 8 ((a) shows the results of case 3; (b) shows the results of case 4).

significant difference in the mixing effect between the two cases, but the results of case 1 (single-phase flow) show locally better than those of case 2 (see the results in the first row and the fifth row in Figure 9). Grace showed experimentally that independent of flow type, the minimum critical capillary number (Ca_{crit}) for droplet breakup is found to be around a viscosity ratio of 1 [12]. It also explains that the single-phase flow with viscosity ratio of 1 between fluid 1 and fluid 2 is more conducive to mixing than the two-phase flow in this work. Furthermore, it can be predicted that with the increasing of rotations, the difference will be more obvious. 10 million particles would cause a huge amount of calculation, and thus we only calculated one rotation.

Figure 10 shows the distributions of particles in the half filled conveying element at different angles in one rotation for case 3 and case 4. In partially filled cases, the particles rarely enter the gap between the screw and the barrel, which

is different from the full filled cases. It is because in the full filled cases, the pressure will press particles into the gap. Obviously, in this work, the particle fluidity in case 3 (single-phase flow) is better than that in case 4 (two-phase flow). It is because in case 4, fluid 1 (3 Pa·s) has a higher viscosity than fluid 2 (1 Pa·s). It also can be found from Figures 10(c)–10(e) that the velocities in the bottom of the left chamber are close to 0 m/s. In the partially filled cases, the maximum velocity appears not only in the intermeshing region but also in the area close to screw flight. It demonstrates that for a partially filled case, the fluid is mainly conveyed under the drag of screw and barrel, while in a full filled case, there is additional effect of pressure pumping.

Figure 11 shows the axial velocity in the cross section of the half filled conveying element during a half of rotation (clockwise rotation). In general, the velocity distributions of the two cases are similar. However, the position of the maximum velocity in the intermeshing region is different. As mentioned earlier, two-phase flow breaks the symmetry of flow field. It also can be found from that the velocities in the bottom of the left chamber are close to 0 m/s.

By observing the mixing processes of case 3 and case 4 in 3 rotations, we found that the difference in viscosity of the two phases is very unfavorable for their mixing, and even some particles would gradually splash out. Figure 12 shows the top view of particle distribution after 3 rotations between the results of case 3 (the left column) and case 4 (the right column). Obviously, in the upper left region of the right figure, a number of red particles have been stripped out. In addition, the interface of the two phases in the right figure is also more irregular compared with the left figure.

Figure 13 shows the comparison of the particle distribution after 3 rotations between the results of case 3 and case 4 corresponding to the 5 cross sections shown in Figure 8. Obviously, there are longer two-phase interfaces in case 3 than in case 4. Some red particles spread out in case 4. In addition, due to the absence of background pressure in the partially filled case, the particles are more inclined to bypass the gap between the two screws.

7. Conclusion

In this work, we used the SPH method to simulate multi-phase flow and mixing in a conveying element of a co-rotating twin-screw extruder. The flow and mixing of two-phase fluids with different viscosity ratio in a full filled or partially filled extruder were studied. We provided a detailed analysis of multiphase flow in a 3D TSE. A two-phase Poiseuille flow was used to validate the effectiveness of SPH. The SPH results showed good agreement with the analytical solution.

SPH is very suitable for simulating multiphase flow in complex industrial machinery. Due to the different parameters of the two-phase fluids, the symmetry of the flow field in the TSE is broken. The difference of viscosity between multiphase fluids is not conducive to blending. Because the particles can bypass the gap, the mixing effect in partially filled cases is not as good as that in full filled cases. For the latter, particles are forced into the gap (especially the gap between screw and screw), which is very conducive to mixing.

In addition, in real polymer extrusion, the heat generated by viscous dissipation within gap cannot be ignored. Moreover, the actual polymer melt is a non-Newtonian fluid. To ensure the calculation accuracy of flow and heat transfer in clearance, a high resolution (small initial particle spacing) is needed. Because very narrow clearance exists in extruders and particles are uniformly arranged in the entire computational domain in the standard SPH, a high resolution will lead to a huge computational cost. This is a limitation of the current algorithm. Therefore, it is very necessary to develop a particle refinement SPH method in the future.

Data Availability

The data used to support the findings of this study are available from the corresponding author upon reasonable request.

Conflicts of Interest

The authors declare that they have no conflicts of interest.

Acknowledgments

References

[1] G. Fourtakas and B. D. Rogers, "Modelling multi-phase liquid-sediment scour and resuspension induced by rapid flows using smoothed particle hydrodynamics (sph) accelerated with a graphics processing unit (gpu)," *Advances in Water Resources*, vol. 92, pp. 186–199, 2016.

[2] X. Zhao, X. Li, and J. Zhang, "Large eddy simulation of multiphase flow and slag entrapment in molds with different widths," *Metals*, vol. 11, no. 2, p. 374, 2021.

[3] H. Tang, L. C. Wrobel, and Z. Fan, "Tracking of immiscible interfaces in multiple-material mixing processes," *Computational Materials Science*, vol. 29, no. 1, pp. 103–118, 2004.

[4] M. H. Kim, W. Szydlowski, J. L. White, and K. Min, "A new model of flow in a tangential counter-rotating twin screw extruder," *Advances in Polymer Technology*, vol. 9, no. 1, pp. 87–95, 1989.

[5] T. Sastrohartono, Y. Jaluria, and M. V. Karwe, "Numerical simulation of fluid flow and heat transfer in twin-screw extruders for non-Newtonian materials," *Polymer Engineering and Science*, vol. 35, no. 15, pp. 1213–1221, 1995.

[6] M. A. Barrera, J. F. Vega, and J. Martínez-Salazar, "Three-dimensional modelling of flow curves in co-rotating twin-screw extruder elements," *Journal of Materials Processing Technology*, vol. 197, no. 1-3, pp. 221–224, 2008.

[7] B. P. Xu, H. W. Yu, and L. S. Turng, "Distributive mixing in a corotating twin screw channel using Lagrangian particle calculations," *Advances in Polymer Technology*, vol. 37, no. 6, pp. 2215–2229, 2018.

[8] A. Khalifeh and J. R. Clermont, "Numerical simulations of non-isothermal three-dimensional flows in an extruder by a finite-volume method," *Journal of Non-newtonian Fluid Mechanics*, vol. 126, no. 1, pp. 7–22, 2005.

[9] X. S. Sun and M. Sakai, "Numerical simulation of two-phase flows in complex geometries by using the volume-of-fluid/ immersed-boundary method," *Chemical Engineering Science*, vol. 139, pp. 221–240, 2016.

[10] G. Pokriefke, "CFD-Analysis of free surface flow inside a twin screw extruder," in *Proceedings of the International Congress on FEM Technology with ANSYS CFX & ICEM CFD Conference*, pp. 61–72, Dresden, Germany, December, 2004.

[11] Z. Chen, Z. Zong, M. B. Liu, L. Zou, H. T. Li, and C. Shu, "An SPH model for multiphase flows with complex interfaces and large density differences," *Journal of Computational Physics*, vol. 283, pp. 169–188, 2015.

[12] V. Pandey and J. M. Maia, "Extension-dominated improved dispersive mixing in single-screw extrusion. Part 1: computational and experimental validation," *Journal of Applied Polymer Science*, vol. 138, no. 4, 2021.

[13] R. A. Gingold and J. J. Monaghan, "Smoothed particle hydrodynamics: theory and application to non-spherical stars," *Monthly Notices of the Royal Astronomical Society*, vol. 181, no. 3, pp. 375–389, 1977.

[14] V. P. Nguyen, T. Rabczuk, S. Bordas, and M. Duflot, "Meshless methods: a review and computer implementation aspects," *Mathematics and Computers in Simulation*, vol. 79, no. 3, pp. 763–813, 2008.

[15] A. J. C. Crespo, J. M. Domínguez, B. D. Rogers et al., "DualSPHysics: open-source parallel CFD solver based on smoothed particle hydrodynamics (SPH)," *Computer Physics Communications*, vol. 187, pp. 204–216, 2015.

[16] A. Ferrari, M. Dumbser, E. F. Toro, and A. Armanini, "A new 3D parallel SPH scheme for free surface flows," *Computers & Fluids*, vol. 38, no. 6, pp. 1203–1217, 2009.

[17] T. Jiang, Y. Tang, and J. Ren, "A corrected 3D parallel SPH method for simulating the polymer free surface flows based on the XPP model," *CMES-Computer Modeling in Engineering and Sciences*, vol. 101, no. 4, pp. 249–297, 2014.

[18] F. He, H. Zhang, C. Huang, and M. B. Liu, "A stable SPH model with large CFL numbers for multi-phase flows with large density ratios," *Journal of Computational Physics*, vol. 453, Article ID 110944, 2022.

[19] T. W. Dong, H. S. Liu, S. L. Jiang, L. Gu, and X. F. Liu, "Simulation of free surface flow with a revolving moving boundary for screw extrusion using smoothed particle hydrodynamics," *Computer Modeling in Engineering and Sciences: Computer Modeling in Engineering and Sciences*, vol. 95, pp. 369–390, 2013.

[20] A. Eitzlmayr and J. Khinast, "Co-rotating twin-screw extruders: detailed analysis of conveying elements based on smoothed particle hydrodynamics. part 1: hydrodynamics," *Chemical Engineering Science*, vol. 134, pp. 861–879, 2015.

[21] P. Wittek, G. G. Pereira, M. A. Emin, V. Lemiale, and P. W. Cleary, "Accuracy analysis of sph for flow in a model extruder with a kneading element," *Chemical Engineering Science*, vol. 187, pp. 256–268, 2018.

[22] T. W. Dong, S. L. Jiang, J. C. Wu, H. S. Liu, and Y. D. He, "Simulation of flow and mixing for highly viscous fluid in a twin screw extruder with a conveying element using parallelized smoothed particle hydrodynamics," *Chemical Engineering Science*, vol. 212, Article ID 115311, 2020.

[23] T. W. Dong, Y. D. He, J. C. Wu, S. Y. Jiang, X. Y. Huang, and X. R. Yan, "Numerical simulation of flow in complex geometries by using smoothed particle hydrodynamics," *Industrial & Engineering Chemistry Research*, vol. 59, no. 40, pp. 18236–18246, 2020.

[24] H. Bauer, J. Matić, and J. Khinast, "Characteristic parameters and process maps for fully-filled twin-screw extruder elements," *Chemical Engineering Science*, vol. 230, Article ID 116202, 2021.

[25] H. Bauer, J. Matić, R. C. Evans et al., "Determining local residence time distributions in twin-screw extruder elements via smoothed particle hydrodynamics," *Chemical Engineering Science*, vol. 247, Article ID 117029, 2022.

[26] T. W. Dong and J. C. Wu, "Simulation of non-Newtonian flows in a partially filled twin-screw extruder by smoothed particle hydrodynamics," *Polymer Engineering and Science*, vol. 62, no. 3, pp. 802–814, 2022.

[27] T. Avalosse and M. J. Crochet, "Finite-element simulation of mixing: 1. Two-dimensional flow in periodic geometry," *AICHE Journal*, vol. 43, no. 3, pp. 577–587, 1997.

[28] J. J. Monaghan and J. C. Lattanzio, "A refined method for astrophysical problems," *Astronomy and Astrophysics*, vol. 149, pp. 135–143, 1985.

[29] J. P. Morris, P. J. Fox, and Y. Zhu, "Modeling low Reynolds number incompressible flows using SPH," *Journal of Computational Physics*, vol. 136, no. 1, pp. 214–226, 1997.

[30] S. Adami, X. Y. Hu, and N. A. Adams, "Transport-velocity formulation for smoothed particle hydrodynamics," *Journal of Computational Physics*, vol. 241, pp. 29–307, 2013.

[31] B. J. Leimkuhler, S. Reich, and R. D. Skeel, "Integration methods for molecular dynamic," in *Mathematical Approaches to Biomolecular Structure and Dynamics*, pp. 161–189, Springer, New York, NY, USA, 1996.

[32] R. A. Dalrymple and O. Knio, "SPH modelling of water waves," in *Proceedings of the Fourth Conference on Coastal Dynamics*, pp. 779–787, Lund, Sweden, August, 2001.

[33] J. Pawlowski, *Die Ähnlichkeitstheorie in der physikalisch-technischen Forschung*, Springer Publishers, Germany, 1971.

[34] M. Robinson, P. Cleary, and J. J. Monaghan, "Analysis of mixing in a Twin Cam mixer using smoothed particle hydrodynamics," *AICHE Journal*, vol. 54, no. 8, pp. 1987–1998, 2008.

[35] S. Leclaire, M. Reggio, and J. Y. Trepanier, "Numerical evaluation of two recoloring operators for an immiscible two-phase flow lattice Boltzmann model," *Applied Mathematical Modelling*, vol. 36, no. 5, pp. 2237–2252, 2012.

[36] V. Everaert, L. Aerts, and G. Groeninckx, "Phase morphology development in immiscible PP/(PS/PPE) blends influence of the melt-viscosity ratio and blend composition," *Polymer*, vol. 40, no. 24, pp. 6627–6644, 1999.